Transverse-Mode Characteristics of GaSb-Based VCSELs With Buried-Tunnel Junctions

Shamsul Arafin, *Member, IEEE*, Alexander Bachmann, *Member, IEEE*,
and Markus-Christian Amann, *Fellow, IEEE*

Abstract—We report the transverse-mode characteristics of GaSb-based vertical-cavity surface-emitting lasers (VCSELs) with buried-tunnel junctions (BTJs). The optical-index guiding in the devices is achieved by an effective refractive index step due to the presence of a laterally structured BTJ in the cavity. All lasing modes in VCSELs of different active diameters are experimentally measured. Then the experimental results are compared against the theoretical data for two different VCSEL designs emitting at 2.3 and 2.6 μm yielding a good agreement. The transverse-mode spacing between the excited modes is also determined and the results are compared with the theory. The far-field patterns ensure that devices with reasonable aperture diameters operate in single-fundamental LP_{01} mode, showing that the devices are well-designed.

Index Terms—Buried-tunnel junction (BTJ), index guiding, mode spacing, transverse mode, vertical-cavity surface-emitting laser (VCSEL).

I. INTRODUCTION

ELECTRICALLY pumped GaSb-based vertical-cavity surface-emitting lasers (VCSELs) operating above 2 μm are of significant interest for gas sensing by tunable diode laser absorption spectroscopy (TDLAS) [1], [2]. In such sensing applications, single transverse-mode operation of VCSELs is one of the key requirements. Despite of the inherent single longitudinal mode behavior, lasing of higher order transverse modes is a common phenomenon in VCSELs with even relatively small active diameters. Due to excitation of several transverse modes, the device is usually no longer suited as laser sources in the targeted applications.

In oxide-apertured index-guided GaAs-based VCSELs, single-mode emission is observed only in very small devices of typically less than 4 μm diameter [3]. In long-wavelength InP-based BTJ VCSELs with molecular beam epitaxy (MBE) regrowth, this transverse single-mode operation has been found for devices with diameter of $\leq$6 μm [4], even though the index guiding of the device is stronger than in GaAs-based VCSEL structures. This is mainly due to the fact that the maximum transverse device dimensions approximately scale with the

wavelength. Therefore, very long wavelength VCSELs above 2 μm will get this benefit even more.

Several attempts have already been made to control the transverse-mode in index-guided VCSELs and single-fundamental mode operation has been achieved from devices with large apertures [5]–[8]. Because a transverse single-mode operation from large-area devices is always beneficial since they promise low differential series and thermal resistance, long lifetime due to low current densities and high output power at small divergence angles.

Single or multimode, continuous or quasi-continuous-wave (CW) electrically pumped (EP) GaSb-based VCSELs emitting at $\sim$2.3 [9], [10] and $\sim$2.6 μm [11], [12] have been demonstrated recently. However, transverse-mode behavior in these devices has not yet been investigated which is the purpose of this paper.

We demonstrate, for the first time, an experimental and theoretical analysis of transverse-mode characteristics for index-guided GaSb-VCSELs. This index guiding is obtained by an effective refractive index step due to the presence of a buried-tunnel-junction (BTJ) concept. Besides index guiding, the BTJ concept also ensures an effective lateral current confinement in the device. At the same time, it allows the substitution of the p-type layers by n-type ones on top of the BTJ to obtain low electrical resistance, and, as a consequence, reduced heat generation in the devices. However, achieving a single transverse-mode operation from GaSb-based BTJ VCSELs with even a small-aperture diameter is a challenging task due to the presence of a strong index guiding behavior. Here, we have experimentally presented how the index guiding can be reduced in the device and such reduction lead to an improvement in terms of a transverse single-mode operation from large-area devices.

This paper is organized as follows. Section II presents the device schematics and a theoretical background of the index guiding mechanism in GaSb-based BTJ VCSELs. The experimental results of the transverse-mode behavior of VCSELs emitting at 2.3 and 2.6 μm will be mentioned in Section III and these results will be compared with theory. The far-field profiles of both types of VCSELs will also be presented there. Finally, Section IV concludes the paper.

II. THEORY

A. Transverse Index Guiding in BTJ VCSELs

A schematic illustration of the MBE-grown GaSb-based BTJ VCSELs is shown in Fig. 1, where D_{BTJ} denotes the aperture diameter of the device. The electric current injected around the dielectric mirror is effectively confined by the structured tunnel junction. As mentioned, this tunnel junction also enables transversal optical index guiding self-adjusted
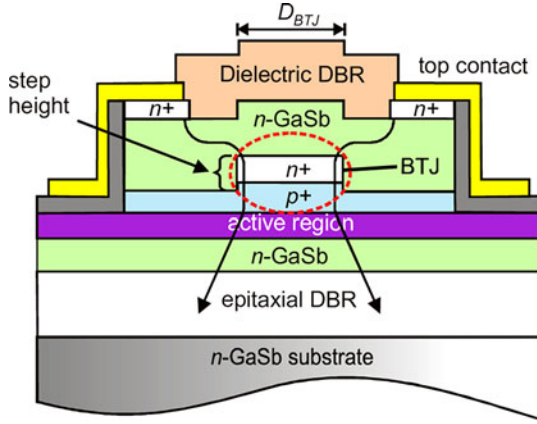
Fig. 1. Schematic cross-sectional view of the GaSb-based VCSEL structure with BTJ. The current path is shown.
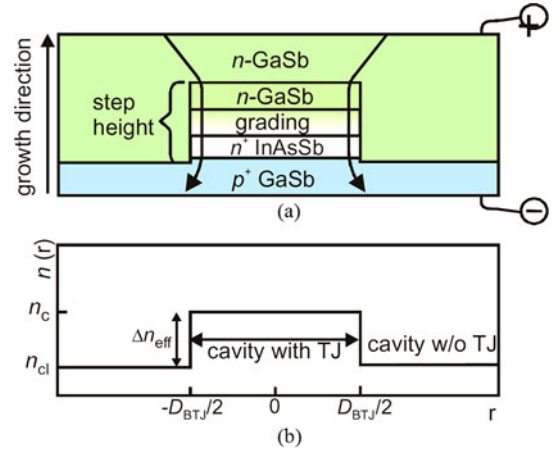

Fig. 2. (a) Magnified view (dashed red-colored circle in Fig. 1) of the tunnel-junction region with current flow in GaSb-based BTJ VCSELs. (b) Index guiding, caused by the step of the BTJ, is illustrated here. Cavity model with step-refractive-index profile $n(r)$.

to the current injection which greatly facilitates the VCSEL fabrication process. The tunnel-junction layers are made of highly doped n^+ InAsSb/p^+ GaSb. Details of the device design and all fabrication steps required to realize the device are given in [13].

The index guiding in BTJ VCSELs mainly arises from a longer cavity in the central region with a tunnel junction aperture rather than in the perimeter. Consequently, a radial index step, Δn_{eff} due to the step height (as shown in Fig. 1 by a dashed red-colored circle) is formed in the tunnel-junction region. Note that the step from the tunnel junction propagates through the entire structure which is clearly seen after the regrowth in MBE. Thus, the step at the interface of the top epitaxially grown GaSb layer and the e-beam evaporated dielectric DBR as well as on top of the dielectric DBR is formed in the device structure, as shown in Fig. 1.

The index-guiding properties can be investigated by using a simple effective index model developed by Hadley [14]. In fact, the laser resonator can be described similar to a step-index glass fiber by using the effective indices in the central part, n_{C} and in the outer part, $n_{\text{Cl}} = n_{\text{C}} - \Delta n_{\text{eff}}$. A theoretical formula relating this induced built-in refractive index step to a shift of the resonator wavelength, $\Delta\lambda$ can be described by [14]

$$\frac{\Delta n_{\text{eff}}}{n_{\text{C}}} = \frac{\Delta\lambda}{\lambda_{\text{C}}} = \frac{\lambda_{\text{C}} - \lambda_{\text{Cl}}}{\lambda_{\text{C}}} \quad (1)$$

where λ_{C} and λ_{Cl} are the resonance wavelengths in the area with tunnel junction and the area without tunnel junction of the VCSEL, respectively. These resonance wavelengths can be evaluated by means of the 1-D transfer-matrix method [15] and the effective refractive index in the tunnel-junction region can be approximated by computing the longitudinally field weighted average refractive index [16]

$$n_c = \sqrt{\frac{\int n^2(z)\,|E(z)|^2\,dz}{\int |E(z)|^2\,dz}} \quad (2)$$

where $E(z)$ is the amplitude of the longitudinal standing wave field, $n(z)$ is the refractive index of each epitaxial layer in the longitudinal direction and the integration is performed from the substrate to the outer boundary of dielectric DBR.

The magnified view of the dotted red-colored circle in Fig. 1 is displayed in Fig. 2, where one can see that the step height is not only due to the n^+-InAsSb layer itself, but also grading layer and n-GaSb layer. This graded junction is introduced between the n^+-InAsSb and the top n-GaSb layers for better electrical conductivity and ohmic characteristics. These grading layers are made of $(Ga_x In_{1-x})$ $(As_y Sb_{1-y})$ with a homogeneously increasing Ga- content and decreasing In-amount.

B. Amount of Index Guiding

The lateral definition of the BTJ is accomplished by etching off the upper n^+-InAsSb, grading and a thin n-GaSb layer and covering the whole structure by an n-GaSb layer in a second epitaxial run. Finally, the total step height in BTJ VCSELs is in the range of 50–70 nm, where the contributions of the above-mentioned n^+ InAsSb, grading and thin n-GaSb layer to the total step height is 20 nm, 10–20 and 20–30 nm, respectively. In fact, this step height referring to the physical length difference between etched and nonetched part is rather high since grading and top n-GaSb layer must be included along with tunnel-junction layer. It is obvious that the higher the etch depth in the tunnel-junction region, i.e., the higher the step height, the higher the index guiding in the device. Fig. 3 shows the degree of the index guiding against the etch depth of the tunnel junction, where Δn_{eff} is calculated by (1) and (2). Note that, throughout the entire discussion of this study, the effective refractive index step, Δn_{eff} caused by the BTJ has been assumed to be the prime reason for index guiding in the device. For the devices presented here, we find constant wavelength spacing between transverse modes independent of driving current hinting that thermal guiding caused by local heating (the refractive index increases with increasing temperature) can be neglected [17]. Antiguiding caused by carrier gradients (high carrier concentrations decrease the refractive index) is also not considered to be a strong effect since the waveguiding property of a strong index-guided VCSEL is not significantly affected by temporal changes in the carrier density [18]. It should also be
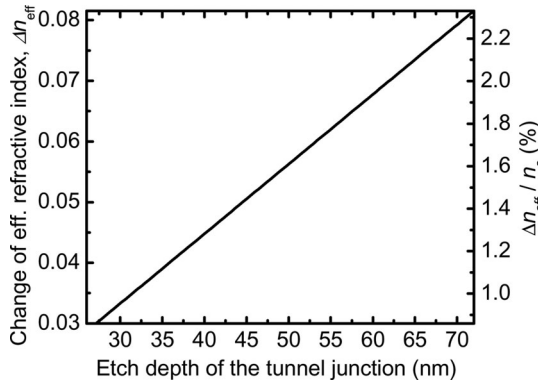
Fig. 3.   Change of the effective refractive index, Δn_{eff} as a function of the etch depth of the tunnel junction.

Fig. 5.   Two-dimensional intensity distribution of the five lowest LPtransverse modes in a VCSEL. Both cos and sin solutions of individual modes are displayed.
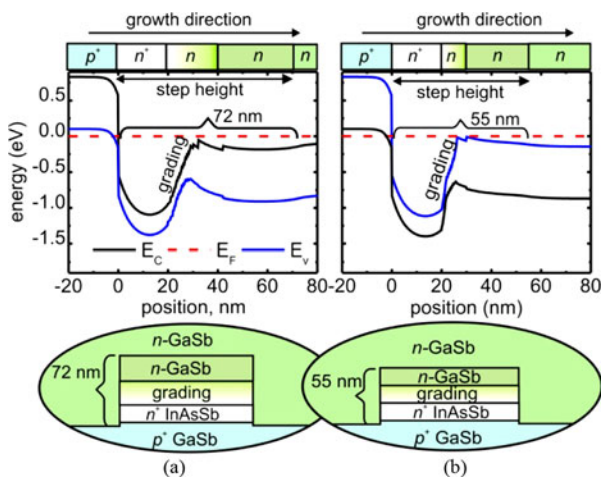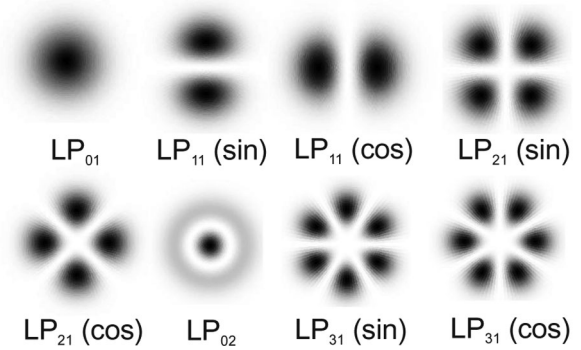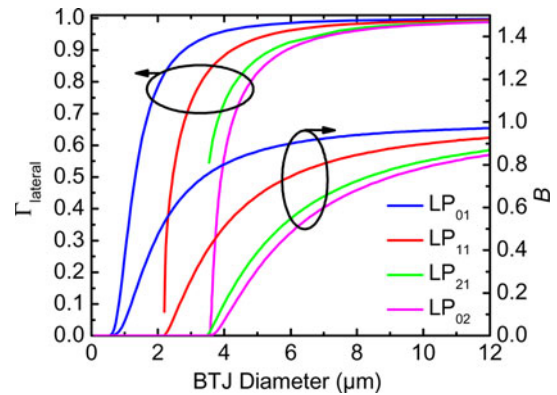

Fig. 4.   Band diagram of tunnel-junction regions in BTJ VCSELs for the emission wavelength of (a) 2.3 μm and (b) 2.6 μm. Both band diagrams have been calculated with SimWindows 1.5.0 [19] using the material parameters from [20].

Fig. 6.   Dependence of the lateral confinement factor, Γ_{lateral} and phase parameter, B on the BTJ diameter of BTJ VCSELs at 2.3 μm for the four lowest LP modes.

mentioned that the presented single-mode VCSELs operate in single mode over the entire operating range.

C. VCSEL Design with Regard to Index Guiding

In this section, we briefly describe the design of 2.3 and 2.6 μm VCSELs with two different degrees of index guiding. In 2.3 μm VCSELs, the relative change of the effective indices calculates to $\Delta n_{\text{eff}}/n_C \approx 2.4\%$, whereas, in 2.6 μm VCSELs, this value amounts to $\Delta n_{\text{eff}}/n_C \approx 1.7\%$, indicating a strong index guiding. This will lead to multimode behavior even for small-aperture diameters.

For 2.3 μm VCSELs, the higher effective index step is due to the use of thick grading layers in the cavity. The thinner grading layer was used in 2.6 μm VCSELs that results in a reduced step height. Fig. 4 illustrates the band diagram of both VCSELs only at the tunnel-junction region, specifically, in the region of the dashed red-colored circle of Fig. 1. It should be noted that the tunnel junction is located at the node of the standing wave pattern in BTJ VCSELs in order to reduce the optical absorption loss, which also helps in obtaining a reduced index guiding in the device.

As mentioned before, the main reason for using grading layers in the cavity is to reduce the InAsSb/GaSb heterointerface resistivity. Importantly, the electrical performance in terms of series resistance of a 10- and 20-nm-thick grading layer was found to be identical. However, the use of such a 20-nm-thick grading layer in the BTJ results in an increased index guiding which has been observed in 2.3 μm VCSELs. Thus a thinner grading layer was introduced in 2.6 μm VCSELs in order to obtain a reduced index guiding. The same reasoning also holds for the thickness of n-GaSb layer.

D. Excited Transverse Modes

Transverse modes of circular-shaped VCSELs can be approximated by linearly polarized (LP$_l$p) modes [21]. The indices l and p are the azimuthal and radial transverse-mode numbers, respectively. In a perfectly circular device, the sine and cosine solutions are degenerate, and thus, the two intensity distributions can arbitrarily be superimposed. Fig. 5 shows the intensity distributions of the five lowest transverse LP$_l$p modes with identical core diameter. In the following discussion, only these five LP modes will be considered for a multimode device though several other higher order modes will appear in that device simultaneously.

The effective gain experienced by a mode can be understood by the lateral confinement factor, Γ_{lateral}, which is plotted in Fig. 6 as a function of BTJ diameter of an BTJ VCSEL at

2.3 μm for the four lowest transverse modes. With increasing diameter, the mode overlap with the core increases and hence does Γ_{lateral}. When no selection mechanism is applied to select a certain transverse mode, the fundamental mode has the highest value of Γ_{lateral}. This parameter is determined by the fraction of the total optical power propagating in the region with BTJ [22]

$$\Gamma_{\text{lateral}} = \frac{\int_0^{D_{\text{BTJ}}/2} |E(r)|^2 \, r dr}{\int_0^\infty |E(r)|^2 \, r dr} \tag{3}$$

where $E(r)$ is the electric field strength in the transverse direction.

The phase parameter or the normalized effective refractive index, B against BTJ diameter is also shown on the right y-axis of Fig. 6. This parameter provides insight into the actual mode distribution via the effective refractive index, n_{eff}. The phase parameter is defined by [22]

$$B = \frac{n_{\text{eff}}^2 - n_{\text{Cl}}^2}{n_{\text{C}}^2 - n_{\text{Cl}}^2}. \tag{4}$$

E. Single-Mode Operation

As mentioned above, VCSEL can be approximated as a cylindrical step-index optical fiber. Knowing the core and cladding refractive indices, it is possible to apply waveguide analysis to find the mode cutoff. The mode cutoff is determined by a normalized frequency parameter, V, which can be represented by the following relation [21]:

$$V = \frac{\pi D_{\text{BTJ}}}{\lambda} \sqrt{n_{\text{C}}^2 - n_{\text{Cl}}^2} \tag{5}$$

where λ is the lasing wavelength. The single-mode condition is simply represented by

$$V < 2.405 \tag{6}$$

where no optical loss is assumed.

By using this single-mode condition, all 2.3 μm VCSELs with $D_{\text{BTJ}} \geq 2.3$ μm and 2.6 μm VCSELs with $D_{\text{BTJ}} \geq 2.5$ μm are supposed to support multiple transverse modes. But, experimentally the devices with larger apertures [compared to the values estimated by (5) and (6)] emit in a single fundamental mode with a reasonable side-mode suppression ratio (SMSR), i.e., >25 dB. Therefore, these devices are "single-mode lasers" as well. As a matter of fact, single-mode lasers may have a laser cavity that supports multiple modes but only the fundamental mode lases. The reason behind this is mode-selective loss in the cavity. In other words, the losses for all excited modes are not same in the cavity of a device, i.e., the loss of higher order modes in single-mode lasers with multimode cavities is too high for gain to compensate, and thus, lasing to occur.

In our BTJ VCSELs, there is a small built-in mode selectivity in terms of the absorption loss and the mirror loss that favors the fundamental LP$_{01}$ mode. Diffraction loss has been proven to be the main mode selecting mechanism in the presented VCSELs due to BTJ-induced topology of top layers [23]. The higher diffraction loss for the higher order modes helps to suppress the higher order modes and thereby improve the single-mode performance. It was found that the diffraction loss rapidly increases below a certain BTJ diameter and even becomes the dominant cause of loss in device with $D_{\text{BTJ}} < 8\mu$m.

F. Transverse-Mode Spacing

The transverse-mode spacing in VCSELs is affected by the aperture diameter, emission wavelength and the index guiding. Compared to GaAs-based VCSELs, GaSb-based BTJ VCSELs for a certain aperture diameter possess larger transverse-mode spacing. Therefore, single-mode operation even in large-aperture GaSb-VCSELs can be easily confirmed from common spectra measurements. The large mode spacing in these devices is just because of the longer emission wavelength and the higher index step caused by the BTJ. The mode spacing, $\Delta\lambda$ between modes LP$_{lp}$ and LP$_{l*p*}$ is [24]

$$\Delta\lambda = |\lambda_{lp} - \lambda_{l*p*}|$$

$$= |2(p^* - p) + (l^* - l)| \frac{\lambda^3}{2\pi^2 w_0^2 n_C^2} \tag{7}$$

where λ is the emission wavelength and w_0 is the spot radius, which is given by

$$w_0 = \frac{D_{\text{BTJ}}}{2\sqrt{\ln(V)}}. \tag{8}$$

Equation (8) is valid for step-refractive-index profile produced in the cavity with tunnel junction. It is not surprising that the combinations of l and p representing LP modes resulting in $\Delta\lambda = 0$ in (7). It means that those modes (e.g., LP$_{21}$ and LP$_{02}$) are frequency degenerated since they have the identical $(2p + l)$ values where for any type of mode profile $(2p + l)$ is the mode group number. [21]. However, in reality, a lack of isotropy in the material or a geometric asymmetry could introduce a lifting of the frequency degeneracy in these modes and give a nonzero $\Delta\lambda$ value.

According to (7), the mode spacing between two adjacent modes is equal and can be written as follows:

$$\Delta\lambda = \lambda_{01} - \lambda_{11} = \lambda_{11} - \lambda_{21}$$

$$= \frac{\lambda^3}{2\pi^2 w_0^2 n_C^2} = \frac{2\lambda^3 \ln(V)}{\pi^2 D_{\text{BTJ}}^2 n_C^2}$$

$$= \frac{2\lambda^3 \ln\left(\frac{\pi D_{\text{BTJ}}}{\lambda} \sqrt{n_C^2 - n_{\text{Cl}}^2}\right)}{\pi^2 D_{\text{BTJ}}^2 n_C^2} \tag{9}$$

It is seen that the mode spacing is proportional to the emission wavelength and the index guiding and inversely proportional to the BTJ diameter of the device. Equation (9) might be used to estimate the effective refractive index difference, $n_C - n_{\text{Cl}}$ from the measured mode spacing and known data of n_C, λ, and D_{BTJ}.

G. Far Fields

When propagating LP$_{01}$-mode distribution, the spot size w_z at a distance z along the beam from the beam waist for a beam of wavelength λ is given by [25]

$$w_z^2 = w_0^2 \left(1 + \frac{z^2}{z_R^2}\right) \tag{10}$$

with the Rayleigh distance z_R of the beam in air, for which
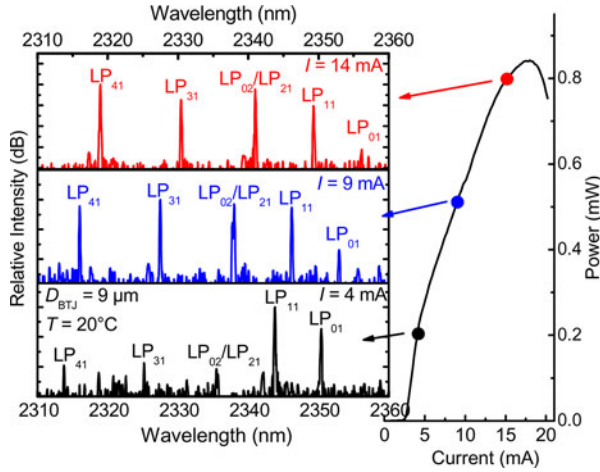
$$z_R = \frac{\pi w_0^2}{\lambda}. \tag{11}$$

Fig. 7. Output characteristic and driving-current-dependent spectra of a BTJ VCSEL at 2.3 μm with an aperture diameter of 9 μm at 4, 9 and 14 mA. The first six transverse modes can be identified. At low currents, LP_{11} is the strongest mode, while at higher currents the higher order modes are dominating. Due to the degeneracy, LP_{21} and LP_{02} are designated as superimposed modes. Similarly, LP_{31} and LP_{12} or LP_{03}, LP_{22} and LP_{41} are degenerated modes which are not mentioned here.

In the far-field approximation, $z \gg z_R$ and using (11), w_z can be written as

$$w_z = \frac{z\lambda}{\pi w_0}. \tag{12}$$

This allows us to specify a formula for the full-width at half-maximum (FWHM) angle

$$\theta_{\mathrm{FWHM}} = 2\sqrt{\ln 2}\tan^{-1}\frac{\lambda}{\pi w_0}. \tag{13}$$

Replacing w_0 by simply $D_{\mathrm{BTJ}}/2$

$$\theta_{\mathrm{FWHM}} \approx 2\sqrt{\ln 2}\tan^{-1}\frac{2\lambda}{\pi D_{\mathrm{BTJ}}}. \tag{14}$$

The approximation of (14) is only valid when $D_{\mathrm{BTJ}} = D_{\mathrm{BTJ,eff}}$, where $D_{\mathrm{BTJ,eff}}$ is the effective BTJ aperture diameter. But, usually $D_{\mathrm{BTJ}} < D_{\mathrm{BTJ,eff}}$ since the lateral current spreading between the BTJ defined current aperture and the active region and also the lateral carrier diffusion in the active region lead to a broadening of the effectively pumped area in the active region.

III. EXPERIMENTAL RESULTS

A. Emission Spectra

Emission spectra of the devices were measured with a Vertex 70 (Bruker Optics GmbH) and a Peltier-cooled extended InGaAs detector. The measured spectral lasing linewidths are limited by the resolution of the Fourier transform infrared spectroscopy (FTIR) system.

Fig. 7 displays the output characteristic and the current-dependent CW spectra of a 9 μm GaSb-based BTJ VCSEL with an emission wavelength of 2.3 μm at a heat sink temperature of 20 °C. The device exhibits multimode operation. Beside the fundamental mode at around 2.35 μm, also LP_{11}, LP_{21}/LP_{02}, LP_{31}/LP_{12}, and $LP_{41}/LP_{03}/LP_{22}$ modes can be identified. The identification of these modes is reported here based on the the-
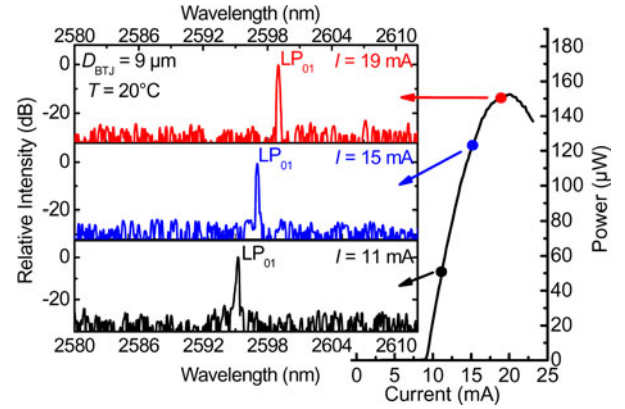

Fig. 8. Output characteristic and spectra of a BTJ VCSEL with an emission wavelength of 2.6 μm at different driving currents and constant heat sink temperature of 20 °C, yielding single-mode operation with a SMSR > 25 dB.

oretical consideration discussed in Section II-F. As can be seen, with increasing current, the higher order mode gets stronger, while the fundamental mode emission gets weaker. Possible reasons are spatial hole burning [26] and inhomogeneous lateral current injection leading to a higher carrier concentration at the borders of the aperture [27].

Output characteristic and current-dependent CW spectra for the VCSEL at 2.6 μm with an aperture diameter of 9 μm at 20 °C are shown in Fig. 8, yielding distinct single-mode emission over the entire operating range. The SMSR is over 28 dB. Note that VCSELs at 2.3 μm with 9 μm aperture exhibit multimode emission, whereas 2.6 μm VCSELs with the same aperture show single-mode emission with a good SMSR. This can be attributed to a reduced refractive index step due to the lower step height in 2.6 μm VCSELs, proves the expected device improvement due to the thinner tunnel junction. Though devices at 2.6 μm get benefited in terms of the single-mode emission from the longer emission wavelength.

B. Mode and Aperture-Diameter-Dependent Resonant Wavelength

The mode-dependent resonant wavelength can be related to the mode-dependent phase parameter, B via [28]

$$\lambda_{lp} = \lambda_{1-D} - \lambda_{1-D}\frac{n_C - n_{Cl}}{\langle n\rangle}(1 - B_{lp}) \tag{15}$$

where λ_{1-D} is the 1-D design wavelength and $<n>$ being the average refractive index of the laser resonator.

Fig. 9 shows the measured (extrapolated) and calculated wavelengths for LP_{01}, LP_{11}, LP_{21}/LP_{02}, and LP_{31} modes against the BTJ diameters of VCSELs at 2.3 μm. These transverse modes are mentioned here since they appear in this order in a VCSEL. For the experimental determination, it has to be taken into account that the devices have different internal heating depending on the aperture diameter and the driving current. Therefore, to compare devices at equal internal heating, several spectra for different bias currents have been measured for all VCSELs. Then, the wavelength of each device has been extrapolated to the hypothetical value at 0 mW heating, as shown in Fig. 10 for a device with 8 μm aperture diameter.
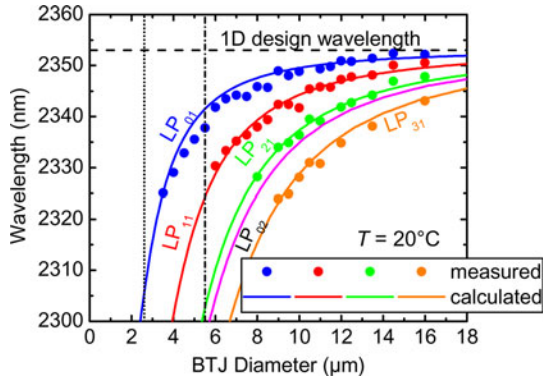
Fig. 9. Measured extrapolated and calculated wavelengths of LP_{01}, LP_{11}, LP_{21}/LP_{02}, and LP_{31} modes according to (15) against BTJ-diameter at 20 °C. Higher order modes are not included here. The horizontal solid line indicates the 1-D design wavelength which is obtained from the 1-D transfer-matrix method. The theoretical (according to (6)) and experimental single-mode cutoff condition in 2.3 μm VCSEL are shown as a vertical dotted line and dashed-dotted line, respectively.
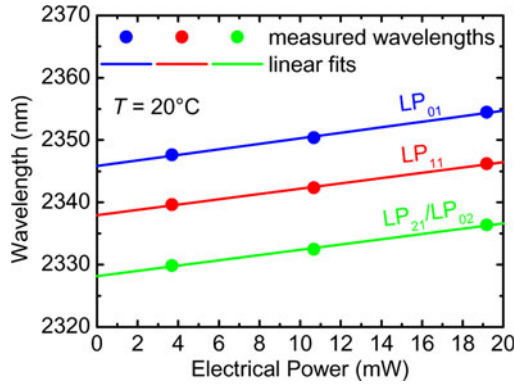

Fig. 10. Wavelengths of LP_{01}, LP_{11}, and LP_{21}/LP_{02} modes for a GaSb-based BTJ VCSEL with 8 μm aperture diameter against applied electrical power at 20 °C. The wavelengths are extrapolated to 0 mW. This hypothetical wavelength is taken for each device in Fig. 9 in order to be able to compare the lasers that have different internal heating under operation.

As known, the lasing wavelength shifts to shorter wavelengths as the transverse cavity dimensions (i.e., BTJ aperture diameter) are reduced. The same behavior is also observed in oxide-apertured VCSELs [16]. The blueshift results because small cavities transform the lasing mode from a plane wave into a true three dimensional mode [29], [30].

The extrapolated wavelengths for the first two LP_{01} and LP_{11} modes against devices with different BTJ diameters are plotted also in Fig. 11 for VCSELs at 2.6 μm. The measured values are in good accordance with the theory. The strong dependence of the emission wavelength on the aperture diameter is due to the strong index guiding in the device and the very long emission wavelength. The design of VCSELs for a specific narrow wavelength range therefore requires considering this effect. On the other hand, on a single wafer VCSELs with single-mode emission wavelength in a range of $\approx$ 10 nm can be realized by applying different aperture diameters in a lithography mask set.

Note that in Figs. 9 and 11, there is an obvious deviation of experimental single-mode cutoff line (dashed-dotted) from the
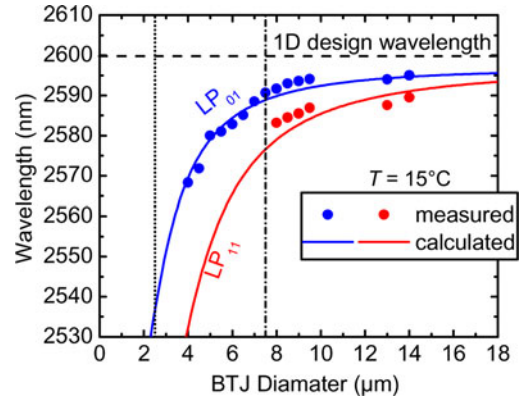

Fig. 11. Measured extrapolated and calculated wavelengths of LP_{01} and LP_{11} modes against BTJ-diameter at 15 °C.
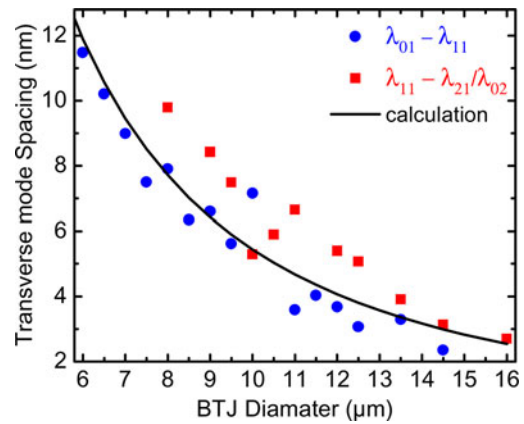

Fig. 12. Wavelength separation between LP_{01} and LP_{11} modes as well as LP_{11} and LP_{21}/LP_{02} modes against BTJ diameters of 2.3 μm VCSEL. The separation between these modes is calculated by using (9).

theoretical line (dotted) in VCSELs under study which is simply due to the aforementioned reason discussed in Section II-E. In addition, the reason for the slight difference between the horizontal dashed line representing 1-D design wavelength and the experimentally measured values representing fundamental LP_{01} mode wavelength can be attributed to the thickness inaccuracies in the epitaxial growth and insufficient knowledge of material data, resulting in a reduced cavity length.

From Figs. 9 and 11, it is worth pointing out that the devices with $D_{BTJ} \leq 5.5$ μm for 2.3 μm VCSELs and $D_{BTJ} \leq 8$ μm for 2.6 μm VCSELs will emit in a single fundamental mode with power at least 25 dB above any higher order modes or noise.

C. Transverse-Mode Spacing

Fig. 12 displays the transverse-mode spacing between the fundamental mode (LP_{01}) and the first higher order mode (LP_{11}) as a function of the BTJ aperture diameter at constant internal heating. It is seen that the mode spacing decreases with increasing active diameter of the device due to the fact that the index difference between two adjacent modes decreases in a large area device. The measured values are in very good agreement with calculated values using (9). Note that, the transverse-mode spacing for a certain aperture diameter in BTJ VCSELs is a bit higher
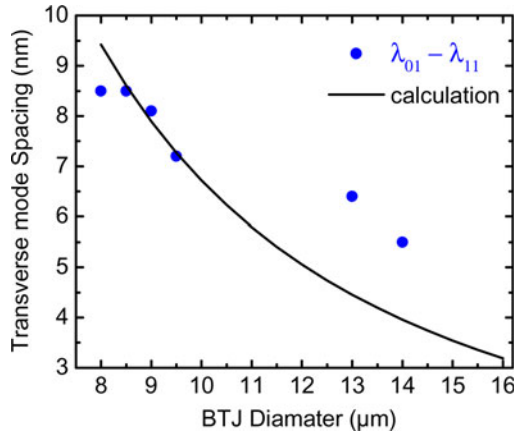
Fig. 13. Wavelength separation between LP_{01} and LP_{11} modes against BTJ diamaters of 2.6 μm VCSEL.

Fig. 14. Measured far field of GaSb-based BTJ-VCSELs at 2.3 μm with an aperture diameter of 4.5 μm at (a) thermal rollover current and (b) VCSELs at 2.6 μm with an aperture diameter of 6 μm at three times threshold current. Both measurements are done at ambient room temperature. The FWHMs far-field angles are $\approx$28° and $\approx$22° for (a) and (b), respectively. Compared to VCSELs at 2.6 μm, the higher value of FWHM angle in 2.3 μm VCSEL is due to the use of a device with a smaller BTJ aperture diameter.

than in GaAs or InP-based VCSELs because of larger emission wavelength and strong index guiding. Measured values are in the range of 2–12 nm, as shown in Fig. 12.

The mode spacing of VCSELs at 2.6 μm is illustrated in Fig. 13. Note that the mode spacing should be somewhat larger in 2.6 μm VCSEL than 2.3 μm VCSEL due to the longer emission wavelength of 2.6 μm VCSEL. However, the long wavelength effect is outbalanced by lower index guiding in 2.6 μm VCSEL as already mentioned. The large deviations between the theoretical and experimental results at large-aperture devices in Fig. 13 are not fully understood yet.

A further comment should be made about the amount of index guiding in the device which can be estimated from the mode spacing. The well-fit of measured value with the theory indicates that the value of index step we have calculated according to (1) and (2) is almost right. In other words, one can easily calculate the value of the BTJ induced step index by (9) by using such experimental data. For instance, with $n_C = 3.4$, $\lambda = 2.35$ μm, and $\Delta\lambda = 9$ nm (the measured wavelength separation between LP_{01} and LP_{11} mode from Fig. 12) for a BTJ-VCSEL of 7 μm aperture diameter emitting at 2.3 μm, the refractive index step, $n_C - n_{Cl}$ can be calculated to be $8 \cdot 10^{-2}$ which is pretty close to $8.2 \cdot 10^{-2}$ we calculated by (1) and (2).

D. Far Fields

Fig. 14 displays full 3-D measured far-field profiles of 2.3 and 2.6 μm GaSb-based BTJ-VCSELs with aperture diameters of 4.5 and 6 μm, respectively. Both measurements were performed at ambient room temperature, in cw-operation and on a system with a computer controlled *xyz*-motorized stage. A Peltier-cooled extended InGaAs detector was kept at a reasonable distance ($\sim$20 cm) from the VCSELs to detect the emitted light. Both devices emit in a single-fundamental LP_{01} mode with a Gaussian intensity distribution. Due to the rotational symmetric Gaussian beam profile, VCSELs are perfectly suited for simple fiber coupling. The y-directional far-field profiles of both devices are also shown in Fig. 14 which exhibits a single-lob pattern with a narrow divergence angle defined by the FWHM angle. These angles are calculated to be 30° and 25° for 2.3 and 2.6 μm VCSELs, respectively, using (14). De-
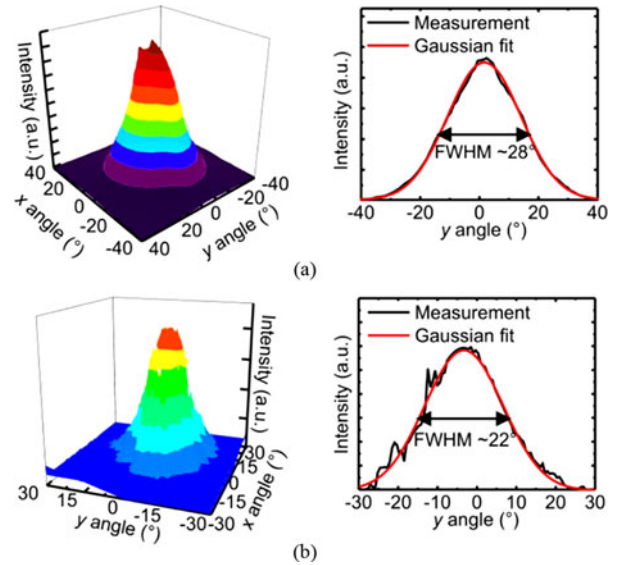
vices have single intensity peaks also in x direction (not shown), revealing single-transverse-mode operating and the good beam quality of the BTJ-VCSEL. It should be noted that, the stronger index guiding in devices under study, compared to GaAs-based oxide-apertured VCSELs, results higher FWHM far-field angles [31], which can be seen in Fig. 14.

IV. CONCLUSION

The transverse-mode characteristics of GaSb-based BTJ VCSELs emitting at 2.3 and 2.6 μm have been extensively studied, both theoretically and experimentally. Such an extensive analysis provides insight into the control of transverse mode of VCSELs under study. VCSELs at 2.6 μm with 9 μm BTJ aperture diameter show single-mode emission over the entire operating range. This single-mode behavior from large-aperture device results from a reduced step height caused by a thinner tunnel junction compared to 2.3 μm VCSELs which eventually lead to a weak optical-index guiding in the device. The analysis also indicates that single-mode behavior from large aperture devices can be further improved with a further reduction of the step height of the tunnel junction. These developments in such an easy control of transverse modes can significantly advance the use of BTJ-VCSELs with greater reliability for a number of sensing applications. Besides, the wavelength splitting between two adjacent modes has been experimentally measured from where one can estimate the amount of index guiding in the device.

REFERENCES

[1] C. Lauer, S. Szalay, G. Boehm, C. Lin, F. Koehler, and M.-C. Amann, "Laser hygrometer using a vertical-cavity surface-emitting laser (VCSEL) with an emission wavelength of 1.84 μm," *IEEE Trans. Instr. Meas.*, vol. 54, no. 3, pp. 1214–1218, Jun. 2005.

[2] P. Werle, F. Slemr, K. Maurer, R. Kormann, R. Mücke, and B. Jänker, "Near- and mid-infrared laser-optical sensors for gas analysis," *Opt. Lasers Eng.*, vol. 37, pp. 101–114, 2002.

[3] B. Weigl, M. Grabherr, C. Jung, R. Jager, G. Reiner, R. Michalzik, D. Sowada, and K. J. Ebeling, "High-performance oxide-confined GaAs VCSELs," *IEEE J. Sel. Topics Quantum Electron.*, vol. 3, no. 2, pp. 409–415, Apr. 2002.

[4] W. Hofmann, C. Chase, M. Müller, Y. Rao, C. Grasse, G. Böhm, M.-C. Amann, and C. J. Chang-Hasnain, "Long-wavelength high-contrast grating vertical-cavity surface-emitting laser," *IEEE Photon. J.*, vol. 2, no. 3, pp. 415–422, Jun. 2010.

[5] Å. Haglund, J. S. Gustavsson, J. Vukusic, P. Modh, and A. Larsson, "Single fundamental-mode output power exceeding 6 mW from VCSELs with a shallow surface relief," *IEEE Photon. Techn. Lett.*, vol. 16, no. 2, pp. 368–370, Feb. 2004.

[6] H. J. Unold, S. W. Z. Mahmoud, R. Jäger, M. Grabherr, R. Michalzik, and K. J. Ebeling, "Large-Area Single-Mode VCSELs and the Self-Aligned Surface Relief," *IEEE J. Sel. Topics Quantum Electron.*, vol. 7, no. 2, pp. 386–392, Mar./Apr. 2001.

[7] H. J. Unold, S. W. Z. Mahmoud, R. Jäger, M. Kicherer, M. C. Riedl, and K. J. Ebeling, "Improving single-mode VCSEL performance by introducing a long monolithic cavity," *IEEE Photon. Techn. Lett.*, vol. 12, no. 8, pp. 939–941, Aug. 2000.

[8] D.-S. Song, S.-H. Kim, H.-G. Park, C.-K. Kim, and Y.-H. Lee, "Single-fundamental-mode photonic-crystal vertical-cavity surface-emitting lasers," *Appl. Phys. Lett.*, vol. 80, no. 21, pp. 3901–3903, 2002.

[9] A. Bachmann, K. Kashani-Shirazi, and M.-C. Amann, "GaSb-based Electrically pumped VCSEL with buried tunnel junction operating continuous wave up to 50 °C," in *Proc. 21 st Intl. Semiconductor Laser Conf. (ISLC 2008)*, paper TuA1, Sep., pp. 39–40.

[10] A. Ducanchez, L. Cerutti, P. Grech, and F. Genty, "Room-temperature continuous-wave operation of 2.3 μm Sb-based electrically pumped monolithic vertical-cavity lasers," *Photon. Technol. Lett.*, vol. 20, pp. 1745–1747, 2008.

[11] S. Arafin, A. Bachmann, K. Kashani-Shirazi, and M.-C. Amann, "Electrically-pumped continuous-wave vertical-cavity surface-emitting lasers at 2.6 μm," *Appl. Phys. Lett.*, vol. 95, pp. 131120-1–131120-3, 2009.

[12] A. Ducanchez, L. Cerutti, P. Grech, F. Genty, and E. Tournié, "Mid-infrared GaSb-based EP-VCSEL emitting at 2.63 μm," *Elec. Lett.*, vol. 45, pp. 265–267, Feb. 2009.

[13] A. Bachmann, S. Arafin, and K. Kashani-Shirazi, "Single-mode electrically pumped GaSb-based VCSELs emitting continuous-wave at 2.4 and 2.6 μm," *New J. Phys.*, vol. 11, pp. 125014-1–125014-18, 2009.

[14] G. R. Hadley, "Effective index model for vertical-cavity surface-emitting lasers," *Opt. Lett.*, vol. 20, no. 13, pp. 1483–1485, 1995.

[15] M. Born and E. Wolf, *Principles of Optics*, 6th ed. Oxford, U.K.: Pergamon Press, 1989.

[16] M. J. Noble, J.-H. Shin, K. D. Choquette, J. A. Lott, and L. Yong-Hee, "Calculation and measurement of resonant-mode blueshifts in oxide-apertured VCSELs," *IEEE Photon. Technol. Lett.*, vol. 10, no. 4, pp. 475–477, Apr. 1998.

[17] M. Brunner, K. Gulden, R. Hövel, M. Moser, and M. Ilegems, "Thermal lensing effects in small oxide confined vertical-cavity surface-emitting lasers," *Appl. Phys. Lett.*, vol. 76, no. 1, pp. 7–9, 2000.

[18] J. Y. Law, "Static, dynamic, and noise characteristics of vertical-cavity surface-emitting lasers," Ph.D. dissertation, School of Eng. and Appl. Sci., Univ. of Rochester, Rochester, NY, 1997.

[19] (1999). SimWindows: Version 1.5.0. Univ. Colorado Boulder [Online]. Available at: http://www.simwindows.com

[20] I. Vurgaftman, J. R. Meyer, and L. R. Ram-Mohan, "Band parameters for III-V compound semiconductors and their alloys," *J. Appl. Phys.*, vol. 89, no. 1, pp. 5815–58751, 2001.

[21] T. Okoshi, *Optical Fibers*, 1st ed. New York: Academic Press, 1982.

[22] D. Gloge, "Weakly guiding fibers," *Appl. Opt.*, vol. 10, pp. 2252–2258, 1971.

[23] J. Bengtsson, J. Gustavsson, Å. Haglund, A. Larsson, A. Bachmann, K. Kashani-Shirazi, and M.-C. Amann, "Diffraction loss in long-wavelength buried tunnel junction VCSELs analyzed with a hybrid coupled-cavity transfer-matrix mode," *Opt. Exp.*, vol. 16, no. 25, pp. 20789–20802, 2008.

[24] K. J. Ebeling, in *Semiconductor Quantum Electronics: From Quantum Physics to Smart Devices*, A. Miller, M. Ebrahimzadeh, and D. M. Finlayson, Eds. Boca Raton, FL: CRC, 1999, pp. 295–338.

[25] B. E. A. Saleh and M. C. Teich, *Fundamentals of Photonics*. New York: Wiley, 1991, ch. 3.

[26] C. Degen, I. Fischer, and W. Elsäßer, "Transverse modes in oxide confined VCSELs: Influence of pump profile, spatial hole burning, and thermal effects," *Opt. Expr.*, vol. 5, no. 3, pp. 38–47, 1999.

[27] C. Lauer, "Antimonid-basierte Vertikalresonator-Laserdioden für Wellenlängen oberhalb 2 μm," Ph.D. dissertation, Walter Schottky Institut, Tech. Univ. Munich, Munich, Germany, 2008.

[28] R. Michalzik and K. J. Ebeling, "Generalized BV diagrams for higher order transverse modes in planar vertical-cavity laser diodes," *IEEE J. Quantum Electron.*, vol. 31, no. 8, pp. 1371–1379, Aug. 1995.

[29] D. G. Deppe and Q. Deng, "Self-consistent eigenmode analysis of the dielectrically-apertured Fabry–Perot microcavity," *Appl. Phys. Lett.*, vol. 71, no. 2, pp. 160–162, 1997.

[30] M. J. Noble, J. P. Loehr, and J. A. Lott, "Analysis of microcavity VCSEL lasing modes using a full-vector weighted index method," *IEEE J. Sel. Topics Quantum Electron*, vol. 34, no. 10, pp. 1890–1903, Oct. 1998.

[31] M. Mochizuki, T. Nishida, S. Kakinuma, and T. Kaneko, "FDTD calculations of the divergence angle of multi-mode VCSELs," in *Proc. SPIE*, 2005, vol. 5722, pp. 201–210.

Shamsul Arafin (M'09) received the B.Sc. degree in electrical and electronics engineering from Bangladesh University of Engineering and Technology, Dhaka, Bangladesh, in 2005 and the M.Sc. degree in communication technology from Universität Ulm, Ulm, Germany, in 2008. He is currently working toward the Ph.D. degree at Walter Schottky Institut, Technische Universität München, Garching, Germany.

His current research interests include GaSb-based vertical-cavity surface-emitting lasers (VCSELs) for wavelengths above 2 μm. He has authored or coauthored more than 20 papers in leading technical journals and international conferences.

Alexander Bachmann (M'07) received the Diploma degree in physics in 2006 from the Technische Universität München, Garching, Germany, where he is currently working toward the Ph.D. degree.

Until 2010, he was a member with the Walter Schottky Institut, Garching, Germany. He has authored or coauthored more than 30 papers in leading technical journals and conferences.

Markus-Christian Amann (A'88–SM'91–F'07) was born in Singen/Hohentwiel, Germany, in 1950. He received the Diploma degree in electrical engineering and the Dr.-Ing. degree from the Technical University of Munich, Munich, Germany, in 1976 and 1981, respectively.

During his thesis work, he studied superluminescent diodes and low-threshold laser diodes, and developed the AlGaAs–GaAs metal-clad ridge-waveguide laser. From 1981 to 1994, he was with the Corporate Research Laboratories, Siemens AG, Munich, where he was engaged in research on long-wavelength InGaAsP–InP laser diodes. In 1990, he became a Deputy Director for the research on laser diodes and integrated optoelectronic devices. On February 1994, he joined the Department of Electrical Engineering at the University of Kassel as a Full professor for "Technical Electronics" establishing a working group for III/V semiconductor electronics and optoelectronics. Since November 1997, he holds the Chair of Semiconductor Technology at the Walter Schottky Institute, Technical University of Munich, where he is currently engaged in research on tunable laser diodes for the near-IR, quantum cascade lasers, long-wavelength vertical-cavity laser diodes, and laser diode applications. He has authored or coauthored some 400 papers and talks (including some 50 invited) on semiconductor optoelectronics in scientific journals, conference proceedings. He has coauthored two books.

Prof. Amann is a member of the German Informationstechnische Gesellschaft (ITG), and a Fellow of the IEEE Lasers and Electro-Optics Society. He has served on numerous conference committees such as the IEEE Semiconductor Laser Conferences, the Indium Phosphide and Related Materials Conferences, and the Conferences on Lasers and Electro-Optics.